## ChemComm



### COMMUNICATION

View Article Online
View Journal | View Issue

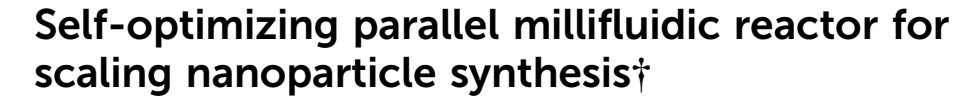


Cite this: Chem. Commun., 2020, 56, 3745

Received 3rd January 2020, Accepted 24th February 2020

DOI: 10.1039/d0cc00064g

rsc.li/chemcomm



Lu Wang, 📭 a Lanja R. Karadaghi, b Richard L. Brutchey 🕩 \* and Noah Malmstadt \* abc

We developed a 16-channel millifluidic reactor that uses a multiphase gas-liquid flow to continuously produce colloidal CsPbBr $_3$  quantum dots with a throughtput of  $\sim 1$  L h $^{-1}$ . The optical properties of the product were monitored, and the reaction conditions were optimized in real time based on the *in situ* photoluminescence characteristics of the quantum dots.

The demand to scale the manufacturing of nanomaterials has been growing, driven by expanding applications in a multitude of industries, such as quantum dot (QD)-based displays. These nanoparticles are typically produced in small-scale batch processes, which are time- and capital-intensive to successfully scale volumetrically. Multiphase segmented-flow micro- and millifluidic reactors (SMRs) are promising platforms for reaction screening processes and the continuous manufacturing of nanomaterials.<sup>2</sup> SMRs possess several advantages over batch reactors, including superior heat and mass transfer inherent in the micro- or milli-dimension channels, excellent reproducibility and control over product quality, reduced environmental health and safety risks, and the capacity for automating reactions.<sup>3</sup> Unfortunately, the throughput of SMRs in a laboratory setting is usually several orders of magnitude lower than the demand for industrial production, hindering the expansion of their application in industry.<sup>4</sup> Moreover, pursuing high-throughput synthesis in SMRs often results in compromised reaction efficiency and quality. For example, enlarging the channel size impairs heat and mass transfer,<sup>5</sup> and increasing the flow rate can result in insufficient residence times, droplet instability, and/or extreme pressure drops in the channels. Alternatively, increasing the number of channels via

There have been previous attempts to parallelize droplet generation in microfluidic systems. Specifically, efforts in synthesizing nanoparticles in parallel reactors have been shown to successfully produce nanoparticles under fixed reaction conditions with a throughput of 10-100 mL h<sup>-1</sup>,7 which is still at least an order of magnitude lower than the throughput needed for industrial production.4 Moreover, these parallel reactors did not adjust reaction conditions in real-time to guarantee product quality and fidelity, which is necessary for an automated scaled-up process. It is therefore essential to integrate in situ process monitoring and feedback control across the parallel network to adjust the reaction conditions accordingly in real time. To accomplish this, we applied in situ spectroscopic detection of product characteristics and chose a "black box" optimization method for feedback control. Black box optimization is faster and more flexible to implement than a more comprehensive modelling approach, facilitating the straightforward implementation of self-optimization across the channel network.8

The reactor described here uses a gas carrier phase to avoid the cost and difficulty of separating and recycling a liquid carrier. Gas/liquid segmented flows offer heat transfer and mixing efficiency advantages similar to the more standard liquid–liquid systems that have dominated the literature. We used this SMR to synthesize CsPbBr<sub>3</sub> perovskite QDs as a model system. The tuneable band gap, high photoluminescence (PL) quantum yields, narrow emission linewidths, suppressed blinking, and high defect tolerance have led to intense interest in these QDs for applications in lasers, LEDs, and photovoltaics. Previous QD flow reactors have used parametric mapping to obtain optimal reaction conditions, but they were not parallelized and they delivered less than 100 mL h<sup>-1</sup> throughput. With the guidance of self-optimized feedback control of *in situ* PL characteristics, we demonstrated a successful synthesis

parallelization is an appealing approach towards achieving a high-throughput synthesis in SMRs as it maintains the reactor geometry for stable production while providing for higher throughput *via* linear scaling. That is, an *n*-channel parallel network leads to an *n*-fold increase in droplet number and an *n*-fold increase in throughput.

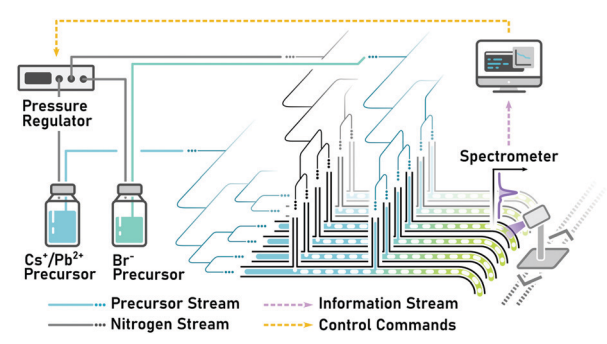
<sup>&</sup>lt;sup>a</sup> Mork Family Department of Chemical Engineering and Materials Science, University of Southern California, 925 Bloom Walk, Los Angeles, California 90089-1211, USA. E-mail: malmstad@usc.edu

<sup>&</sup>lt;sup>b</sup> Department of Chemistry, University of Southern California, 840 Downey Way, Los Angeles, California 90089-0744, USA. E-mail: brutchey@usc.edu

<sup>&</sup>lt;sup>c</sup> Department of Biomedical Engineering, University of Southern California, 3650 McClintock Avenue, Los Angeles, California 90089-1111, USA

 $<sup>\</sup>dagger$  Electronic supplementary information (ESI) available. See DOI: 10.1039/d0cc00064g

Communication ChemComm



Scheme 1 Schematic of the reactor system. The CsPbBr<sub>3</sub> perovskite QD synthesis is distributed in 16 parallel channels and monitored by feedback control based on in situ measured PL characteristics.

of CsPbBr<sub>3</sub> QDs under optimized conditions in a parallel 16-channel millifluidic reactor yielding a throughput of  $\sim 1 \text{ L h}^{-1}$ .

The batch synthesis of CsPbBr3 QDs was originally achieved by swiftly adding a solution of tetraoctylammonium bromide (TOAB) dissolved in toluene into a pre-mixed Cs(oleate) and Pb(oleate)<sub>2</sub> precursor solution in toluene at room temperature with rapid stirring. Under these conditions, cuboidal CsPbBr3 QDs are formed within several seconds.12 This synthesis was adapted for our reactor such that the Cs<sup>+</sup>/Pb<sup>2+</sup> precursor solution (1:1 mol/mol) in toluene was delivered into the reactor with nitrogen gas segmentation, and the Br - precursor solution in toluene was merged with the Cs<sup>+</sup>/Pb<sup>2+</sup> precursor slugs (to give a mole ratio of Cs<sup>+</sup>: Pb<sup>2+</sup>: Br<sup>-</sup> near 1:1:3) to allow for mixing, nucleation, and particle growth while flowing downstream through the millichannels (Scheme 1).

A pressure-driven method for precursor delivery was chosen because it allows for arbitrarily large reagent reservoirs and is appropriate for large-scale processes. The 3D-printed manifold has one inlet and four outlets, evenly distributing fluid with a binary tree structure. Liquid or gas was delivered into one manifold and then distributed into four downstream manifolds, ultimately splitting the flow into 16 channels. To keep comparable flow resistances across the branch channels, identically large flow resistances in each channel were applied to make resistance variance negligible.<sup>13</sup> Polyether ether ketone (PEEK) tubing with inner diameters below 200 µm were used to create large flow resistances at each outlet of the secondary manifolds (Fig. S2, ESI†). Inlet filters were installed to remove solids. Gas/liquid slug generation and stream merging took place in PEEK T-junctions and the reaction occurred in translucent polytetrafluoroethylene (PTFE) tubing (inner diameter = 794  $\mu$ m). Slug behavior and in situ PL spectra of the QD product were monitored through this PTFE tubing (Fig. 1). An infrared (IR) emitter and receiver were clamped across each PTFE channel to monitor slug flow (Fig. S3, ESI†), with changes in receiver voltage corresponding to the fluid passing by the emitter/receiver pair and gas having a greater IR transmittance than liquid (Fig. 1b).14

UV-vis absorbance and PL spectra were collected in situ and used to evaluate the quality of CsPbBr<sub>3</sub> QDs. A 405 nm LED and a deuterium-halogen lamp routed to the flow tubing were alternatively shuttered on and off. Light emitted from the liquid

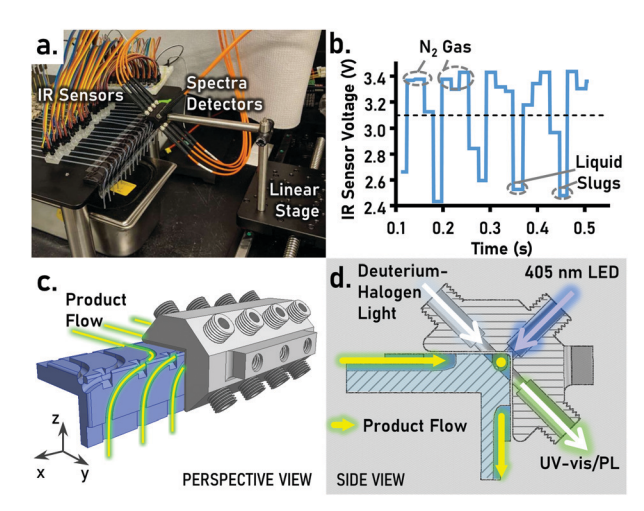


Fig. 1 In situ detection modules. (a) Photograph of the detection system monitoring slugs and PL spectra. (b) Slug status was acquired via IR sensors. Diagrams of the UV-vis/PL detection unit in (c) perspective view and (d) side view

in the tubing upon LED illumination was then analyzed to produce a PL emission spectrum while the light transmitted upon lamp illumination was used to produce a UV-vis spectrum (Fig. 1d). The PTFE tubing was bent in the detection module by 90 degrees in the x-direction, so that light passes through the radial direction of the tubing, minimizing optical interference from the PTFE (Fig. 1c and d). The detection module consisted of four optical channels and was translated through the 16 reactor channels via a linear stage (Movie S1, ESI†). Within the detection module, an optical switch (Fig. S4, ESI†) connected light signals from one channel to the spectrometer, while physically blocking the light from the other three channels that are not being read. The channels were read out serially.

The slugs formed across the 16 channels were similar in both frequency and size (Movie S2, ESI†). At optimized driving pressures, the velocities of the slugs were determined to be uniform based on analysis of high-speed video (Fig. S5, ESI†). At driving pressures of 400 mbar (Cs<sup>+</sup>/Pb<sup>2+</sup>), 400 mbar (gas), and 300 mbar (Br<sup>-</sup>), slug frequencies throughout the 16 channels had a mean value of 11 Hz and a coefficient of variance lower than 22% (Fig. S6a, ESI†). Under these fixed driving pressures, 20 slugs were recorded in a single channel and 360 slugs were recorded in all parallel channels with the IR sensors. Comparing the size distributions, slugs had an average residence time in the detector around 50 ms with a coefficient of variance ranging from 29% in a single channel to 35% across the parallel channels. These variations are likely due to the compressibility of the segmenting gas. Since the slug size distribution from a single channel does not significantly differ from that measured across all 16 parallel channels (as evaluated by a Kolmogorov-Smirnov test, Fig. 2a), parallelization does not introduce any significant irregularities in slug formation in this parallel network, which is borne out by consistent QD quality across the parallel network (vide infra).

During the continuous CsPbBr<sub>3</sub> QD synthesis, PL emission maxima ( $\lambda_{\text{max}}$ ) were typically detected in the range of 495–520 nm Parallel Channels

Single Channel

ChemComm

001

Slug Size (ms/drop)

# Fig. 2 Parallelization of $CsPbBr_3$ QD synthesis in the 16 channels. (a) Box plot and histogram showing size distributions of slugs recorded across 16 parallel channels (grey, top) and in a single channel (green, bottom). (b) Normalized offset UV-vis (dotted lines) and PL spectra (solid lines) of the $CsPbBr_3$ QD product in the 16 channels were highly similar.

450

500

Wavelength (nm)

550 600

with full widths at half maximum (FWHMs) varying from 25–45 nm, depending on flow rates and flow rate ratios of precursors and segmenting gas. The emission peak wavelengths across the 16 channels were typically within a variance of 10 nm and FWHMs were within 5 nm difference. At driving pressures of 400 mbar for the Cs<sup>+</sup>/Pb<sup>2+</sup> precursor, 300 mbar for the Br<sup>-</sup> precursor, and 400 mbar for segmenting gas, an example of the UV-vis and PL spectra across 16 parallel channels is presented in Fig. 2b and Table S2 (ESI†). To demonstrate the importance of optimal parallel across the distributed network, the reactor was run at suboptimal conditions and shown to produce inconsistent product (Fig. S6 and S7, ESI†).

To automate CsPbBr<sub>3</sub> QD production with desired quality, a feedback control scheme was established based on the Nelder-Mead black box optimization algorithm, a widely employed simplex algorithm.<sup>15</sup> Our optimization was based on the PL characteristics of the CsPbBr3 QDs, with the goal of maintaining the characteristic narrow FWHM of the CsPbBr<sub>3</sub> QDs, as well as minimizing the FWHM deviation across the 16 channels. To meet the criteria of Nelder-Mead method, where only one optimization goal is sought, we characterized the distribution of FWHMs in 16 channels and set the upper endpoint of the 95% confidence interval (UCI) as the minimizing goal. The input variables are the driving pressures of Cs<sup>+</sup>/Pb<sup>2+</sup> precursors, Br<sup>-</sup> precursor, and segmenting N2 gas. The optimization was accomplished with the boundary conditions being that pressures should not exceed 1 bar (to maintain slug stability), and that driving pressures for the two precursor solutions should avoid extreme differences in stoichiometry (less than a 6:1 mole ratio of Br to Cs /Pb2+ precursor). Within 20 min (allowing for 10 iterations), the optimization reached convergence around 35 nm FWHM (Fig. 3a and b), and a threshold of 35 nm was set to terminate the optimization.

The robustness of the self-optimization process was tested in terms of the ability to recover to optimum conditions following a purposefully introduced disturbance. The flow resistance in the

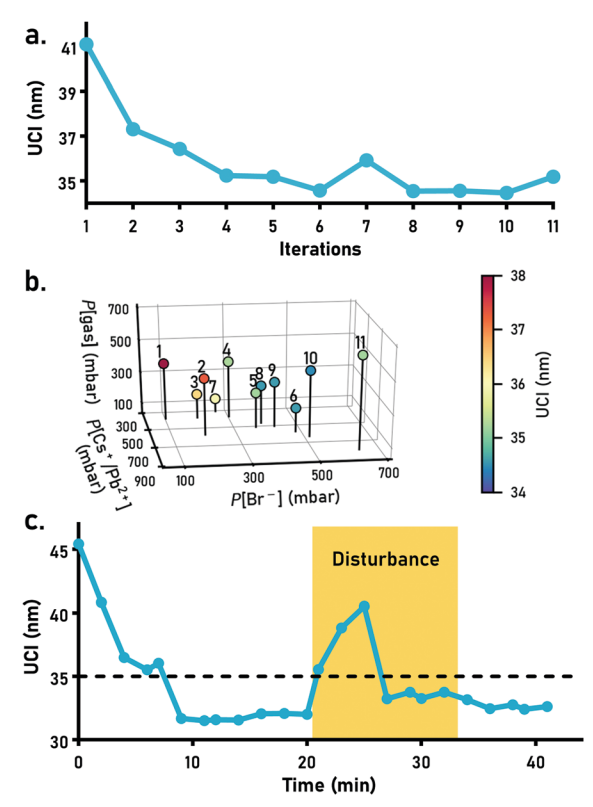


Fig. 3 Self-optimization performance. The goal of self-optimization was set to minimize the upper endpoint of the 95% confidence interval (UCI) in the distribution of FWHMs from the 16 channels. The driving pressures of  $Cs^+/Pb^{2+}$  precursor,  $Br^-$  precursor, and  $R_2$  segmentation gas are denoted as  $R[Cs^+/Pb^{2+}]$ ,  $R[Br^-]$ , and  $R[Br^-]$ , respectively. (a) The search for minimal UCI reached convergence within 8–10 iterations (2 min per iteration). (b) Three variable input pressures across 11 optimization iterations (labeled 1–11) are plotted with a colormap indicating the corresponding UCI. (c) The optimization system stabilized the reactor after a flow disturbance was introduced, and the target UCI below 35 nm was reached again by feedback control despite the disturbance.

Br<sup>-</sup> precursor stream was manually increased to simulate a situation in which debris is caught by the inlet filter. As shown in Fig. 3c, the algorithm initiated a new optimization round when the UCI exceeded 35 nm, and the UCI returned below 35 nm within 3 iterations.

To further demonstrate the reactor stability, we operated the system for an extended duration. The throughput varied from 700 mL h<sup>-1</sup> to 1200 mL h<sup>-1</sup> depending on the size of precursor bottles and flow resistance. In a 4 h reaction, approximately 2.8 L of product was obtained (Fig. 4a). Based on a calculated isolated yield of 80% after workup (based on Cs<sup>+</sup>/Pb<sup>2+</sup>), we can obtain a throughput 1.9–3.2 g h<sup>-1</sup> of CsPbBr<sub>3</sub> QDs in this 16-channel reactor. The slug behaviours and FWHMs in the 16 channels were maintained throughout the entire process (Fig. 4c–e). The resulting CsPbBr<sub>3</sub> QD product from the 16 channels was pooled and collected for *ex situ* characterization after each hour. The UV-vis and PL spectra showed excellent consistency, with narrow PL FWHMs ranging from 21–23 nm (Fig. 4b). Powder X-ray diffraction (XRD) analysis from each time point agreed with the expected orthorhombic structure for

Communication ChemComm

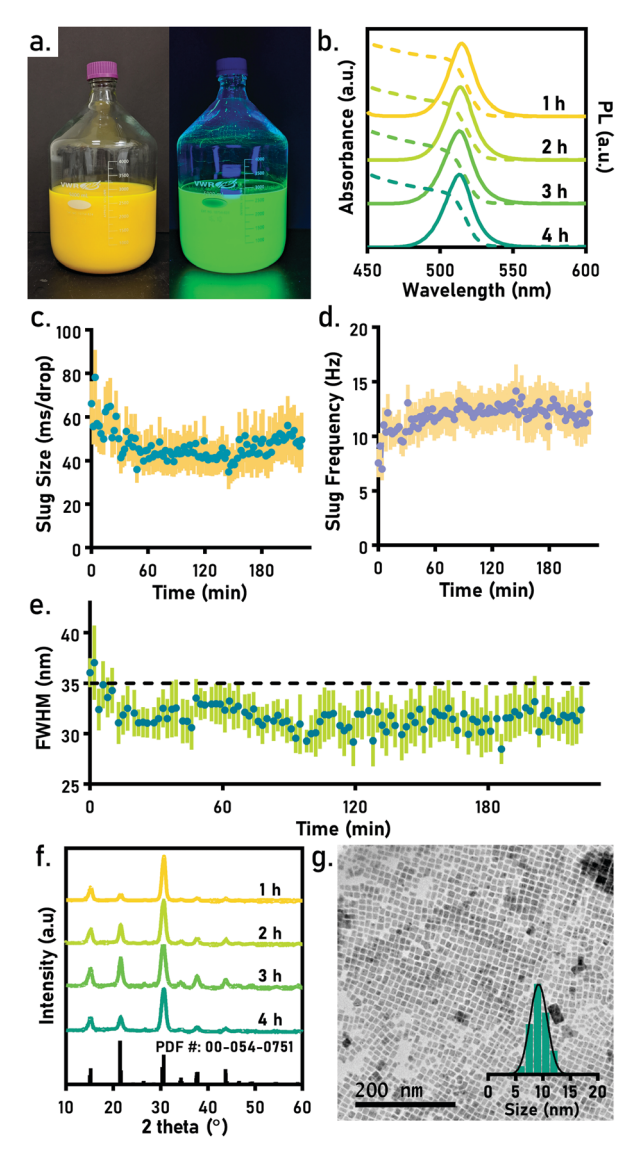


Fig. 4 Reactor performance in an extended automated operation. (a) Photos of collected product in a 5 L bottle from a 4 h synthesis under indoor light (left) and UV light (right). (b) Off-line UV-vis spectra (dotted lines) and PL spectra (solid lines) of product collected from 1-4 h time points. In situ (c) slug sizes, (d) slug frequencies, and (e) FWHMs along the 16 channels are stable throughout the 4 h reaction. The mean values and 95% confidence intervals are plotted in the graphs. (e) Powder XRD of CsPbBr3 QDs obtained at each hour. (f) TEM of CsPbBr3 QDs at 4 h time point, with size distribution given as an inset.

CsPbBr<sub>3</sub> (PDF# 00-054-0751), which confirms a consistent crystal structure of the resulting QDs.16 The TEM images of the pooled product from 1, 2, 3, and 4 h showed consistent average sizes of 9.9  $\pm$  1.6 nm, 10.2  $\pm$  1.7 nm, 9.7  $\pm$  1.7 nm, and 9.4  $\pm$  1.5 nm, respectively (Fig. 4g and Fig. S8, ESI†), which

match the QD sizes obtained from PL data. Energy dispersive X-ray spectroscopy analysis yielded an average ratio of 1:0.92:3.30 for Cs:Pb:Br across the parallel channels (Table S3, ESI†).

In summary, we have successfully developed a parallelized 16-channel automated reactor for the scaled-up synthesis of colloidal CsPbBr<sub>3</sub> QDs. The reactor self-optimizes for product quality based on in situ monitoring of the optical properties of QDs as they are synthesized. This represents the first demonstration of high-throughput nanomaterial synthesis in a feedback-controlled continuous flow parallel reactor. With excellent chemical resistance, highly parallel slug generation, robust optimization algorithms, and a high throughput of approximately 1 L h<sup>-1</sup>, this reactor can be employed broadly towards the scaled-up production of photoluminescent QDs.

This work is supported by the National Science Foundation (grant CMMI-1728649).

### Conflicts of interest

There are no conflicts to declare.

#### References

- 1 M. J. Pitkethly, Mater. Today, 2004, 7, 20-29.
- 2 (a) I. Lignos, R. Maceiczyk and A. J. deMello, Acc. Chem. Res., 2017, 50, 1248-1257; (b) G. Niu, A. Ruditskiy, M. Vara and Y. Xia, Chem. Soc. Rev., 2015, 44, 5806-5820.
- 3 E. J. Roberts, L. R. Karadaghi, L. Wang, N. Malmstadt and R. L. Brutchey, ACS Appl. Mater. Interfaces, 2019, 11, 27479-27502.
- 4 T. W. Phillips, I. G. Lignos, R. M. Maceiczyk, A. J. deMello and J. C. deMello, Lab Chip, 2014, 14, 3172-3180.
- 5 R. L. Hartman, J. P. McMullen and K. F. Jensen, Angew. Chem., Int. Ed., 2011, 50, 7502-7519.
- 6 (a) T. Nisisako, T. Ando and T. Hatsuzawa, Lab Chip, 2012, 12, 3426-3435; (b) S. Yadavali, D. Lee and D. Issadore, bioRxiv, 2019, 625277.
- 7 (a) A. M. Nightingale, J. H. Bannock, S. H. Krishnadasan, F. T. F. O'Mahony, S. A. Haque, J. Sloan, C. Drury, R. McIntyre and J. C. deMello, J. Mater. Chem. A, 2013, 1, 4067-4076; (b) C. T. Riche, E. J. Roberts, M. Gupta, R. L. Brutchey and N. Malmstadt, Nat. Commun., 2016, 7, 10780.
- 8 C. Mateos, M. J. Nieves-Remacha and J. A. Rincón, React. Chem. Eng., 2019, 4, 1536-1544.
- 9 A. Günther, M. Jhunjhunwala, M. Thalmann, M. A. Schmidt and K. F. Jensen, Langmuir, 2005, 21, 1547-1555.
- 10 S. A. Kulkarni, S. G. Mhaisalkar, N. Mathews and P. P. Boix, Small Methods, 2019, 3, 1800231.
- 11 (a) R. W. Epps, K. C. Felton, C. W. Coley and M. Abolhasani, Lab Chip, 2017, 17, 4040-4047; (b) I. Lignos, S. Stavrakis, G. Nedelcu, L. Protesescu, A. J. deMello and M. V. Kovalenko, Nano Lett., 2016, **16.** 1869-1877
- 12 S. Wei, Y. Yang, X. Kang, L. Wang, L. Huang and D. Pan, Chem. Commun., 2016, 52, 7265-7268.
- 13 C. Guermonprez, S. Michelin and C. N. Baroud, Biomicrofluidics, 2015, 9, 054119.
- 14 K. C. Bhargava, B. Thompson and N. Malmstadt, Proc. Natl. Acad. Sci. U. S. A., 2014, 111, 15013.
- 15 J. A. Nelder and R. Mead, Comput. J., 1965, 7, 308-313.
- 16 P. Cottingham and R. L. Brutchey, Chem. Commun., 2016, 52, 5246-5249.